

Effect of isotope on state-to-state dynamics for reactive collision reactions $O(^3P) + H_2^+ \rightarrow OH^+ + H$ and $O(^3P) + H_2^+ \rightarrow OH + H^+$ in ground state $1^2A''$ and first excited $1^2A'$ potential energy surfaces*

Juan Zhao(赵娟)^{1,†}, Ting Xu(许婷)², Lu-Lu Zhang(张路路)¹, and Li-Fei Wang(王立飞)¹

¹School of Science, Shandong Jiaotong University, Jinan 250357, China

²School of Physics and Electronics, Shandong Normal University, Jinan 250358, China

(Received 8 November 2019; revised manuscript received 4 December 2019; accepted manuscript online 24 December 2019)

We carry out quantum scattering dynamics and quasi-classical trajectory (QCT) calculations for the $O + H_2^+$ reactive collision in the ground ($1^2A''$) and first excited ($1^2A'$) potential energy surface. We calculate the reaction probabilities of $O + H_2^+(v=0, j=0) \rightarrow OH^+ + H$ and $O + H_2^+(v=0, j=0) \rightarrow OH + H^+$ reaction for total angular momentum $J=0$. The results calculated by QCT are consistent with those from quantum mechanical wave packet. Using the QCT method, we generate in the center-of-mass frame the product state-resolved integral cross-sections (ICSs); two commonly used generalized polarization-dependent differential cross-sections (PDDCSs), $(2\pi/\sigma)(d\sigma_{00}/d\omega_k)$, $(2\pi/\sigma)(d\sigma_{20}/d\omega_k)$; and three angular distributions of the product rotational vectors, $P(\theta_r)$, $P(\phi_r)$, and $P(\theta_r, \phi_r)$. We discuss the influence on the scalar and vector properties of the potential energy surface, the collision energy, and the isotope mass. Since there are deep potential wells in these two potential energy surfaces, their kinetic characteristics are similar to each other and the isotopic effect is not obvious. However, the well depths and configurations of the two potential energy surfaces are different, so the effects of isotopic substitution on the integral cross-section and the rotational polarization of product are different.

Keywords: quasi-classical trajectory, state-to-state, isotopic substitution, rotational polarization of product

PACS: 31.15.xv, 34.50.-s, 03.67.Lx

DOI: 10.1088/1674-1056/ab6554

1. Introduction

Ion–molecule reactions are attracting increasing attention because they appear in many interesting situations, including interstellar chemistry,^[1] planetary ionospheres, and high-energy physics. Many gas-phase chemical reactions involving ionic species have been well studied experimentally, and a large number of kinetic data have been obtained.^[2] On the theoretical side the dynamical simulations of various reaction systems have been performed.^[3,4]

Researchers have studied theoretically and experimentally the $O+(4S) + H_2$ reaction and fragmentation mechanism of the system^[5–9] and several systems with the form of XH_2^+ ($X = He, Ne, etc.$).^[10–13] However, except for the experimental work reported by McClure *et al.* in 1977,^[14] few reports can be found on the reactive collisions, which include the proton transfer reaction ($OH^+ + H$) for the ground potential energy surface (PES) ($1^2A''$) and the H atom transfer ($OH^+ + H$) reaction for the first excited PES ($1^2A'$). In 2014, the ground ($1^2A''$) and first excited ($1^2A'$) potential energy surfaces of the reactive system have been calculated by Paniagua *et al.*^[15] The $1^2A''$ PES and the $1^2A'$ PES are based on *ab initio* multi-reference configuration interaction calculations^[16,17] by using the augmented correlation-consistent polarized-valence quadruple zeta basis set of Dunning. Using these fitted PESs,

many theoretical studies have been done. Paniagua *et al.*^[15] conducted quasi-classical trajectory (QCT) calculations and obtained integral cross-sections and thermal rate constants of reactions $O(^3P) + H_2^+ \rightarrow OH^+ + H$ and $O(^3P) + H_2^+ \rightarrow OH + H^+$, and their deuterium variants (D_2^+ and HD^+). The results showed that the $O(^3P) + H_2^+$ reaction is mainly controlled by an indirect mechanism in a collision energy range 0 eV–0.5 eV. The reaction that happens in the ground $1^2A''$ PES has a rate constant of tripled rate of the reaction that happens on the excited $1^2A'$ PES, and this value is independent of the isotopic variant. In 2015, Gamallo *et al.*^[18] performed Born–Oppenheimer and Renner–Teller time-dependent quantum dynamics calculations, including the Coriolis coupling (CC) for the reactive collisions $O(^3P) + H_2^+ \rightarrow OH^+ + H$ and $\rightarrow OH + H^+$. Their work is useful for estimating the influence of the non-adiabatic effects. The difference in integral cross-section results from CC and QCT methods and is very small, implying that quantum effects are of little importance in these reactions. The QCT method can be used to study the dynamics of the $O(^3P) + H_2^+ \rightarrow OH^+ + H$ and $O(^3P) + H_2^+ \rightarrow OH + H^+$ reaction. Using these PESs^[15] fitted by Paniagua *et al.*, other research groups have studied $OH^+ + H$ channel. The Meng group^[19] calculated the reaction probabilities and integral cross-section of the $O(^3P) + H_2^+ \rightarrow OH^+ + H$ reac-

*Project supported by the National Natural Science Foundation of China (Grant No. 11504206) and the Shandong Jiaotong University PhD Research Start-up Fund, China.

†Corresponding author. E-mail: zhaajuan@sdjtu.edu.cn

tion and studied the effect of vibrational and rotational excitation of the reactant by using the time-dependent quantum wave packet through using the split operator method. Zhang *et al.*^[20] studied the time-dependent quantum dynamics of the $O(^3P) + D_2^+ \rightarrow OD^+ + D$ for the ground $1^2A''$ PES, and obtained the initial-state-resolved reaction probabilities, integral cross-sections (ICSs), and rate constants. Martínez *et al.*^[21] used the real wave packet (RWP) method to calculate the cross-sections and used the QCT method to investigate the scalar properties (cross-sections, average fractions of energy, and product vibrational distributions) and vector properties of the $O + H_2^+$ reaction for the $1^2A''$ and $1^2A'$ PESs, and to determine the microscopic reaction mechanism (direct mechanism and complex mechanism).

These studies of the $O(^3P) + H_2^+ \rightarrow OH^+ + H$ and $\rightarrow OH + H^+$ reaction mainly focused on the state-to-state in all reaction dynamics. When two molecules collide, the study of the state-to-state reaction dynamics can reveal more detailed observables and provide a profound insight into the chemical reaction process. So it is very necessary to carry out state-to-state calculations for the $O(^3P) + H_2^+ \rightarrow OH^+ + H$ and $\rightarrow OH + H^+$ reactions. In addition, the isotope effect plays a significant role in deducing the chemical reaction mechanics and in determining the intermolecular interaction.^[22,23] Due to the abundance of D (deuterium) in nature, a great deal of research related to the isotopic reaction systems has been done, which revealed some pronounced isotope effects on the scalar and vector properties of certain elementary reactions.^[24–27] To the best of our knowledge, little research has been done in $O(^3P) + H_2^+ \rightarrow OH^+ + H$ and $\rightarrow OH + H^+$ isotopic reactions. In this study, we carry out the QCT calculations to investigate the isotope effects of these reactions.

The rest of this paper is organized as follows. In Section 2, we introduce the theoretical method used in this work. In Section 3, we present the results and discuss some results. And finally, in Section 4 we draw some conclusions from the present study.

2. Methods

2.1. Time-dependent wave-packet method

The general theory of the time-dependent wave packet method has been very perfect and standard,^[28–30] and this method mainly includes three steps. The first step is to construct the initial Gaussian wave packet that can be written as the product of the motion wave packet and initial vibration eigenfunction. The second step is to solve the time-dependent Schrödinger equation ($i\hbar \frac{\partial \psi}{\partial t} = \hat{H} \psi$) by using the reactant Jacobi coordinates through the split-operator scheme as follows:

$$\begin{aligned} & \psi(R, r, t + \Delta) \\ &= e^{-iH_0\Delta/2} e^{-iV_{\text{rot}}\Delta/2} e^{-iV\Delta} e^{-iV_{\text{rot}}\Delta/2} e^{-iH_0\Delta/2} \psi(R, r, t), \quad (1) \end{aligned}$$

$$H_0 = -\frac{\hbar^2}{2\mu_R} \frac{\partial^2}{\partial R^2} - \frac{\hbar^2}{2\mu_r} \frac{\partial^2}{\partial r^2} + V(r), \quad (2)$$

$$V = \frac{(\hat{J} - \hat{j})^2}{2\mu_R R^2} + \frac{\hat{j}^2}{2\mu_r r^2}. \quad (3)$$

The third step is to extract the dynamic information from the final wave packet after a long propagation time. The total reaction probability can then be calculated by

$$P = \sum_j \frac{\hbar}{\mu_r} \text{Im} \left[\langle \psi_j(E) | \delta(s - s_0) \frac{\partial}{\partial s} | \psi_j(E) \rangle \right]. \quad (4)$$

More details of the method can be found in the references therein. The following parameters are used to obtain the converged results of $O(^3P) + H_2^+ \rightarrow OH^+ + H$ reaction: 320 translational basis functions for the R coordinate in a range of $0.5a_0$ – $22.0a_0$, 290 vibrational basis functions for the r coordinate of $1.0a_0$ – $25.0a_0$, $j_{\text{max}} = 160$ for rotational basis functions, and a propagation time of 4.5×10^4 a.u.; For $O(^3P) + H_2^+ \rightarrow OH + H^+$ reaction, 283 translational basis functions for the R coordinate in a range of $0.1a_0$ – $25.0a_0$, 183 vibrational basis functions for the r coordinate in a range of $0.5a_0$ – $20.0a_0$, $j_{\text{max}} = 130$ for rotational basis functions, and a propagation time of 5.0×10^4 a.u. In order to obtain the converged results, many test calculations on each parameter are performed.

2.2. Quasi-classical trajectory method

The quasi-classical trajectory method (QCT) falls within the framework of classical mechanics; quantum numbers are artificially introduced to describe the ends of the trajectory, that is, the reactants and products are described by quantum mechanics, but the propagation of the trajectory over time is obtained by solving the classical Hamilton equation. This method is simple, intuitive, and computationally effective. Because of its relative accuracy, it has been applied to many chemical reactions and has become an important means to study the dynamics of molecular reactions. The initial conditions are obtained by Monte Carlo sampling, and then a large number of trajectories are calculated. Finally, we can obtain a series of dynamic information, such as the reaction probability, integral cross section, product energy distribution, vibrational and rotational distribution, spatial angular distribution, and rotational orientation. In particular, by analyzing the process of trajectory propagation over time, we can intuitively observe the internal mechanism of the reaction. Although the QCT method has achieved great success, it also has some insurmountable shortcomings. For example, quantum tunneling, product zero-point energy (ZPE) vibration, and transition state resonance, cannot be easily dealt with by using the QCT method. Therefore, for systems with obvious quantum effects, the results from the QCT calculation often differ from the actual results. As Davidsson said,^[31,32] the cross sections of the reaction and the close complex formation as a function

of the diatom rotational quantum number are much closer to each other at lower energy without considering ZPE, which indicates a much smaller recrossing phenomenon. So, starting with the traditional QCT method,^[33,34] some improvement has been made. Bonnet and Rayez^[35] developed the Gaussian Binning method, where each trajectory is weighted with a Gaussian-like coefficient, so that it can round-off the product vibrational actions to their nearest integer. Varandas developed the trajectory binning scheme and studied the non-active treatment of zero-point energy leakage.^[36] Therefore, the QCT method is becoming increasingly useful. For some elementary reactions with no obvious quantum effect and heavy multi-atom reaction systems, the QCT method can better describe the motion of atoms on the potential energy surface, and it has a strong advantage in mechanism analysis.

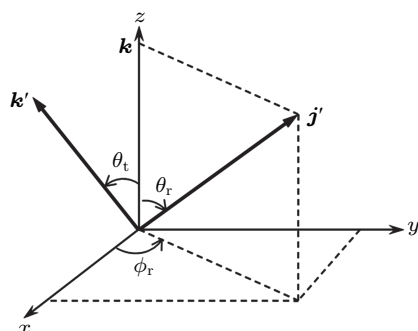


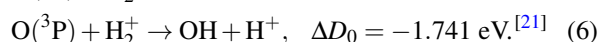
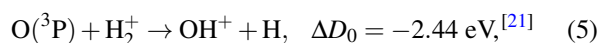
Fig. 1. Center-of-mass coordinate system used to describe k , k' , and j' distribution.

In the present work the calculation method for the QCT is cited from Han's group method, which has been widely used to study both the scalar and the vector properties of the many reactions.^[37,38] The classical Hamilton's equations are numerically integrated in three dimensions. Figure 1 shows the center-of-mass (CM) frame used in this work, the reagent relative velocity vector k is parallel to the z axis and the x - z plane is the scattering plane containing the initial and final relative velocity vector, k and k' . The angle is the scattering angle between the reagent relative velocity and the product relative velocity. and are the polar and azimuthal angles of the final rotational angular momentum j' . In the present work 10^5 trajectories are run for each reaction. The initial distance from the Oxygen atom to the center of mass of H_2^+ (D_2^+/T_2^+) is 15.0 Å, and the integration step size in the trajectories is chosen to be 0.1 fs, which guarantees the conservation of the total energy and total angular momentum. The impact parameter, b_{\max} , is computed by calculating 10^5 trajectories at a fixed value of the impact parameter b and also by systematically increasing the value of b until no reactive trajectories are obtained. The reaction cross section is defined as $\sigma = \pi b_{\max}^2 (N_r/N)$, where N_r is the number of reactive trajectories and N is the total number of trajectories. The initial rotational quantum number and the vibrational quantum number of the reactant are set to be $j = 0$

and $v = 0$. For comparison with the $J = 0$ resulting from the quantum method, the maximum collision parameter (b_{\max}) is set to be 0. The truncated numbers used in the following expansions of $P(\theta_r)$, $P(\phi_r)$, and $P(\theta_r, \phi_r)$, and PDDCSs are 18, 24, and 7, respectively.

3. Results and discussion

This system leads to proton transfer, $OH^+ + H$, on the ground PES and to hydrogen atom transfer, $OH + H^+$, on the first excited PES, with both reaction channels being exoergic and the two PESs being barrier-less and presenting a deep minimum



It can be seen that $OH^+ + H$ channel releases more energy than $OH + H^+$ channel. Figure 2 shows the minimum energy paths^[15] (MEP) for both reactions. For the ground PES ($1^2A''$) there is a deep well (around 8.16 eV below the $O + H_2^+$ reactant) with a nearly T-shaped geometry (the oxygen atom inserts in between the two hydrogen atoms and $(H-O-H)^+$ angle is about 110°); for the excited PES ($1^2A'$) there is also an insertion deep well, but it is about 0.63 eV higher in energy than that for the ground state^[15] and it has an angle near a collinear $(O-H-H)^+$ geometry. But the comparison of energy among products shows that the depth of the potential well in the excited PES is deeper than that in the ground PES (around 5.68 eV for $1^2A''$ and 5.92 eV for $1^2A'$).

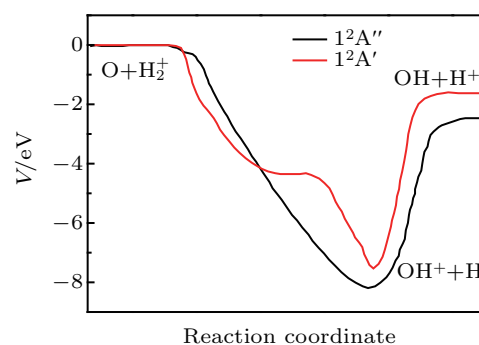


Fig. 2. Reaction path model of $1^2A''$, and potential energy surface of $1^2A'$ in $O + H_2^+$ reactive system.^[15]

3.1. Integral cross section

Figure 3 shows for $J = 0$, total reaction probabilities versus collision energy in a range of 0.01 eV–1.0 eV for $O(^3P) + H_2^+ \rightarrow OH^+ + H$ ($1^2A''$, ground state) and $O(^3P) + H_2^+ \rightarrow OH + H^+$ ($1^2A'$, the first excited state). The solid curve and dotted curve are the quantum results, and the scatter represents the QCT reaction probabilities for the $OH^+ + H$ and $OH + H^+$ product channels, respectively. It can be seen that the reaction possibilities do not present any threshold, this is because of barrier-less MEP and exothermicity; and for $J = 0$, where the centrifugal barrier is equal to zero, the reactions

have no threshold energy. Moreover, one important feature of both the quantum reaction possibilities is the appearance of a very rich pattern of narrow quantum resonances. This resonance structure suggests the existence of an indirect insertion mechanism, favored by the deep minima of both PESs. The difference between both reaction probabilities can also be seen in Fig. 3. In the low-energy region (0.01 eV–0.20 eV) there is little difference between both results, but as the collision energy increases, the gap between the two reaction probabilities turns bigger, that is, the result of $\text{OH}^+ + \text{H}$ channel is larger than that of $\text{OH} + \text{H}^+$ channel. This result can be attributed to two factors: one is the shallower potential well (relative product energy) in the ground state, *i.e.*, compared with the excited state, the ground state has a small barrier to overcome and is easier to produce products; and the other is more exothermic for the ground state, *i.e.*, the lower the energy of the $\text{OH} + \text{H}^+$, the more stable the state is and the bigger the probability on the ground state. In addition for $J = 0$ the QCT reaction probability can be observed to have no resonance structure, and the value is close to the quantum mechanical (QM) one within the entire collision energy range, proving the validity of our QCT calculations.

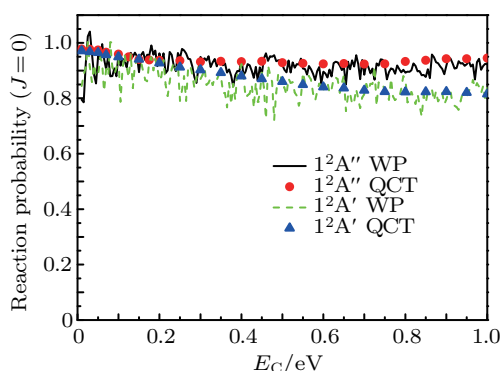


Fig. 3. Plots of total reaction possibility versus E_C for $J = 0$, obtained by TDWP and QCT methods for $\text{O} + \text{H}_2^+ \rightarrow \text{OH}^+ + \text{H}$ on the $1^2A''$ PES and $\text{O} + \text{H}_2^+ \rightarrow \text{OH} + \text{H}^+$ on the $1^2A'$ PES.

In order to compare with previous reaction cross sections, the integral cross sections are also calculated by using the QCT

method. In Fig. 4, the pink line shows the QCT results from this work, and the other results are cited from Ref. [21]. In Fig. 4, it can be seen that our QCT results accord with the ones calculated by Martínez *et al.*[21] By comparing the RWP–CS result with the RWP–CC results it can be seen that the Coriolis coupling effect is not obvious; the comparison of cross section between the RWP and QCT methods shows that the QCT method is accurate enough to study the dynamics of the reactions.

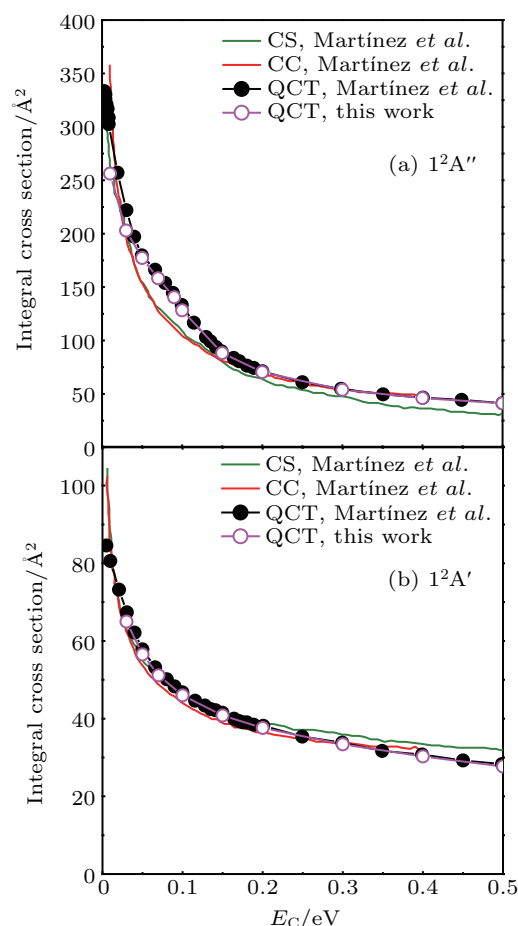


Fig. 4. Cross sections for reactive collision $\text{O} + \text{H}_2^+(0,0)$: (a) on $1^2A''$ PES, and (b) on $1^2A'$ PES, respectively.

Table 1. QCT integral reaction cross section values (without electronic term (2/18)) of reactions of $\text{O} + \text{H}_2^+ \rightarrow \text{OH}^+ + \text{H}$, $\text{O} + \text{D}_2^+ \rightarrow \text{OD}^+ + \text{D}$, $\text{O} + \text{T}_2^+ \rightarrow \text{OT}^+ + \text{T}$ on $1^2A''$ PES and $\text{O} + \text{H}_2^+ \rightarrow \text{OH} + \text{H}^+$, $\text{O} + \text{D}_2^+ \rightarrow \text{OD} + \text{D}^+$, $\text{O} + \text{T}_2^+ \rightarrow \text{OT} + \text{T}^+$ on $1^2A'$ PES.

E_C/eV	$1^2A''$ PES $\sigma/\text{Å}^2$			$1^2A'$ PES $\sigma/\text{Å}^2$		
	$\text{O} + \text{H}_2^+$	$\text{O} + \text{D}_2^+$	$\text{O} + \text{T}_2^+$	$\text{O} + \text{H}_2^+$	$\text{O} + \text{D}_2^+$	$\text{O} + \text{T}_2^+$
0.01	254.825	262.404	267.387	72.934	73.439	73.454
0.03	200.399	203.586	205.701	59.355	60.031	60.369
0.05	174.456	176.937	178.594	50.123	52.131	52.200
0.07	152.653	156.114	157.239	46.871	47.189	47.388
0.09	128.348	132.655	134.819	43.731	43.887	44.115
0.1	117.235	119.308	121.788	42.356	42.706	42.889
0.15	85.992	86.235	86.494	37.962	38.127	38.023
0.2	70.292	70.314	70.479	34.967	34.909	34.685
0.3	54.017	54.147	54.330	31.064	30.486	29.798
0.4	45.770	45.972	46.085	28.257	27.091	26.264
0.5	40.596	40.642	40.743	25.926	24.451	23.335

Table 1 shows the integral cross sections for both the first [Eq. (5)] and second [Eq. (6)] reactions including their isotopic reactions. Here the cross section values are not multiplied by the electronic term (2/18). Some differences can be clearly seen in this table. For the ground state by substituting D and T for H, over the whole collision energy range the cross sections increase constantly which are in the following order: $\sigma(\text{O} + \text{T}_2^+) > \sigma(\text{O} + \text{D}_2^+) > \sigma(\text{O} + \text{H}_2^+)$. But for the excited state when the collision energy is lower, the order of the cross sections turns into $\sigma(\text{O} + \text{T}_2^+) > \sigma(\text{O} + \text{D}_2^+) > \sigma(\text{O} + \text{H}_2^+)$, when the collision energy is higher than 0.15 eV, the order of the cross section becomes $\sigma(\text{O} + \text{T}_2^+) < \sigma(\text{O} + \text{D}_2^+) < \sigma(\text{O} + \text{H}_2^+)$, with σ being the integral cross section calculated by the QCT method.

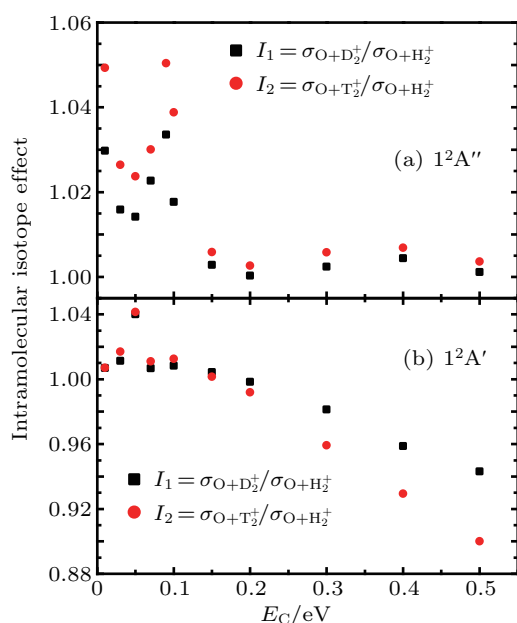


Fig. 5. Collision energy-dependent intramolecular isotope effect ($I_1 = \sigma_{\text{O}+\text{D}_2^+}/\sigma_{\text{O}+\text{H}_2^+}$ and $I_2 = \sigma_{\text{O}+\text{T}_2^+}/\sigma_{\text{O}+\text{H}_2^+}$) on (a) $1^2A''$ PES and (b) $1^2A'$ PES.

Figure 5 shows the intramolecular isotope effect on both states and is defined as $I_1 = \sigma_{\text{O}+\text{D}_2^+}/\sigma_{\text{O}+\text{H}_2^+}$ and $I_2 = \sigma_{\text{O}+\text{T}_2^+}/\sigma_{\text{O}+\text{H}_2^+}$. It can be seen that there is a different isotope effect on the integral cross-sections of the reactions in the $1^2A''$ and $1^2A'$ state. I_1 and I_2 on the ground state have values between 1.0 and 1.05 over the whole investigated energy range, and $I_1 < I_2$ at each collision energy; the same feature exists only in a range of 0.01 eV–0.15 eV for the excited state. When the energy is larger than 0.15 eV, both I_1 and I_2 for the $1^2A'$ state are both smaller than 1.0; and it is true that I_1 is larger than I_2 at each collision energy. These results suggest quite different isotope behaviors for the two states. The formation of the products OT^+ and OD^+ are slightly favored over that of OH^+ for the ground state, while the OH product formation is favored over the OD^+ and OT^+ formation for collision energy larger than 0.15 eV in the excited state. This

can be attributed to the difference in zero-point energy (ZPE). There are also many articles that have reported this isotope effect,^[26,39–46] and these studies show that an important reason for the discrepancy among these results lies in the difference in ZPE. After D and T substitute for H the zero-point energy values of both the reagent molecular ion and the complex are changed, resulting in different shapes of the effective minimum energy path in the entrance channel. By considering the more attractive character of the ground PES (see the equipotential contour plots in Ref. [15]), and the different configurations of the potential well ($R_{\text{HH}} = 1.596 \text{ \AA}$, $R_{\text{OH}} = 0.997 \text{ \AA}$, $\angle [\text{H}-\text{O}-\text{H}]^+ = 106.3^\circ (1^2A'')$ versus $R_{\text{HH}} = 2.034 \text{ \AA}$, $R_{\text{OH}} = 1.016 \text{ \AA}$, $\angle [\text{H}-\text{O}-\text{H}]^+ = 180.0^\circ (1^2A')$), we surmise that the zero-point energy correction at the $[\text{D}-\text{O}-\text{D}]^+$ ($[\text{T}-\text{O}-\text{T}]^+$) potential well is “deeper” than $[\text{H}-\text{O}-\text{H}]^+$ for the ground state and the opposite situation occurs in the excited state.

3.2. Product state distributions

In this subsection, the product state distributions calculated by the QCT method are discussed. Figure 6 shows the product vibrational state distributions for the $\text{O} + \text{H}_2^+/\text{D}_2^+/\text{T}_2^+ \rightarrow \text{OH}^+ + \text{H}$, $\text{OD}^+ + \text{D}$, $\text{OT}^+ + \text{T}$ in the ground $1^2A''$ PES and $\text{O} + \text{H}_2^+/\text{D}_2^+/\text{T}_2^+ \rightarrow \text{OH} + \text{H}^+$, $\text{OD} + \text{D}^+$, $\text{OT} + \text{T}^+$ in the excited $1^2A'$ PES. In Fig. 6, it can be seen that the $\text{OH}^+(v')$ vibrational distributions present the obvious population inversion for $\text{O} + \text{H}_2^+ \rightarrow \text{OH}^+ + \text{H}$ reaction, while it looks that when $v' = 1$ the population reaches a maximum value for each E_C and then monotonically decreases for $\text{O} + \text{H}_2^+ \rightarrow \text{OH} + \text{H}^+$ reaction, which is similar to the result reported in Ref. [21]. Martínez *et al.*^[21] attributed these results to being due to the larger exoergicity [$-2.48 \text{ eV} (1^2A'')$ versus $-1.61 \text{ eV} (1^2A')$] of the ground PES and the smaller vibrational frequency of the corresponding diatomic products [$\text{OH}^+(3116 \text{ cm}^{-1})$ versus $\text{OH}(3696 \text{ cm}^{-1})$]. In Fig. 6, the influence of the isotope substitution on vibrational distribution can also be seen, that is, it gives rise to a broader QCT distribution as expected due to the major proximity of the vibrational levels of the OD^+/OT^+ (OD/OT) product molecule (e.g., at $E_C = 0.1 \text{ eV}$, and the population can reach up to 10, i.e., $v'_{\text{max}} = 10$ for OH^+ , $v'_{\text{max}} = 13$ for OD^+ and $v'_{\text{max}} = 15$ for OT^+ in the ground state PES; $v'_{\text{max}} = 4$ for OH , $v'_{\text{max}} = 6$ for OD , and $v'_{\text{max}} = 7$ for OT in the excited state PES). When an atom in a molecule is replaced by its isotope, the charge distribution of the molecule is not affected, so the force constant does not change. But when D or T substitutes for H, the vibrational frequency of the molecule decreases, and the vibrational energy level of the product molecule, which can be reached, becomes larger.

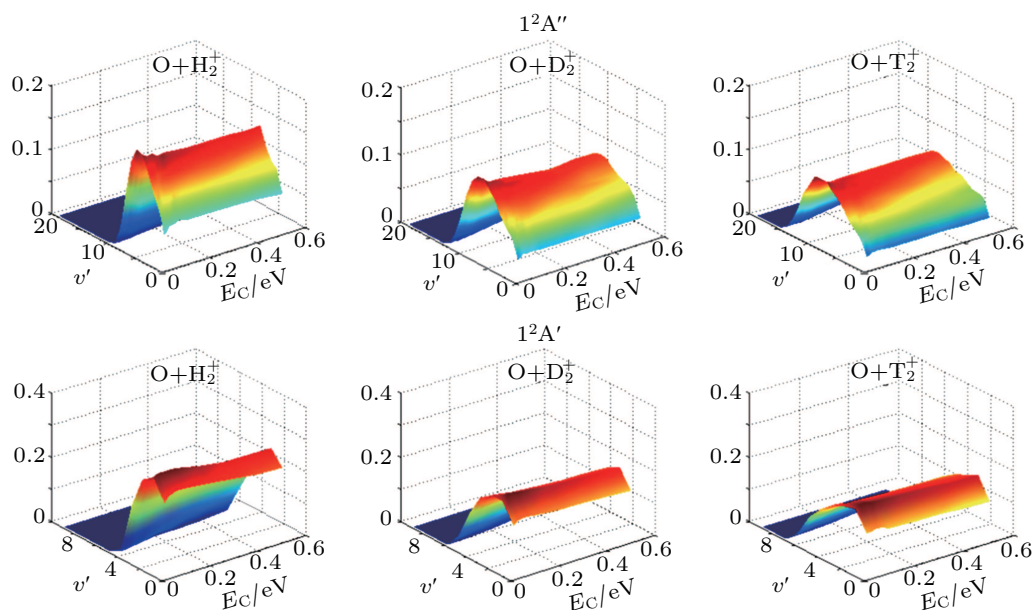


Fig. 6. Product vibrational state distributions for $\text{O} + \text{H}_2^+/\text{D}_2^+/\text{T}_2^+ \rightarrow \text{OH}^+ + \text{H}$, $\text{OD}^+ + \text{D}$, $\text{OT}^+ + \text{T}$ reactions on the $1^2\text{A}''$ PES (upper), and $\text{O} + \text{H}_2^+/\text{D}_2^+/\text{T}_2^+ \rightarrow \text{OH} + \text{H}^+$, $\text{OD} + \text{D}^+$, $\text{OT} + \text{T}^+$ reactions on the $1^2\text{A}'$ PES (lower).

Similarly, the rotational distributions are also examined (Fig. 7). It is clear that the rotational distribution population shows the arch-shape in each case, that is, the rotational states of the product are inverted, which is consistent with the complex-forming mechanism of the reaction. It can be attributed to the heavy light-light (HL-L) mass combination which leads to the fact that the reactant orbital angular momentum L can easily transfer into the product rotation angular momentum j' ; therefore, the rotational distribution has a quantum number inversion. In addition, these results may also be exothermic.^[47] In view of more energy released in the $\text{O} + \text{H}_2^+ \rightarrow \text{OH}^+ + \text{H}$ than in the $\text{O} + \text{H}_2^+ \rightarrow \text{OH} + \text{H}^+$ [$\Delta D_0 = -2.44 \text{ eV}(1^2\text{A}'')$ versus $\Delta D_0 = -1.741 \text{ eV}(1^2\text{A}')$], the ground PES rotational distributions are “hotter” than the excited PES

ones. Besides, the bent configuration of the potential well ($R_{\text{HH}} = 1.596 \text{ \AA}$, $R_{\text{OH}} = 0.997 \text{ \AA}$, $\angle[\text{H}-\text{O}-\text{H}]^+ = 106.3$) in the ground PES may be another important reason for the “hotter” rotational distribution. For $\text{A} + \text{BC} \rightarrow \text{AB} + \text{C}$ class of reaction, when the reaction occurs (B–C bond breaks), the reaction system takes a bent configuration, which makes the repulsive energy released from B–C bond more easily converted into rotational energy, or, the initial orbital angular momentum L more easily converted into the product rotational angular momentum j' . Moreover, when D and T substitute for H, the rotational distribution becomes broader and broader, and the peak becomes shorter and wider. This can be attributed to the relatively small rotational level spacing in OD^+/OT^+ (OD/OT).

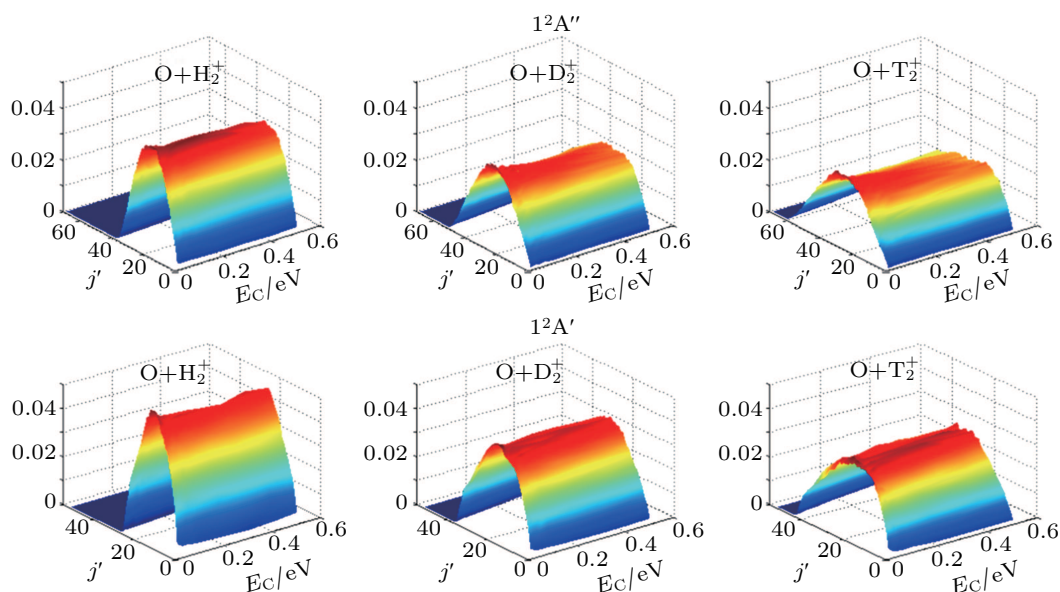


Fig. 7. Product rotational state distributions for $\text{O} + \text{H}_2^+/\text{D}_2^+/\text{T}_2^+ \rightarrow \text{OH}^+ + \text{H}$, $\text{OD}^+ + \text{D}$, $\text{OT}^+ + \text{T}$ reactions on the $1^2\text{A}''$ PES (upper), and $\text{O} + \text{H}_2^+/\text{D}_2^+/\text{T}_2^+ \rightarrow \text{OH} + \text{H}^+$, $\text{OD} + \text{D}^+$, $\text{OT} + \text{T}^+$ reactions on the $1^2\text{A}'$ PES (lower).

In order to more intuitively display the state distribution of product molecule, we plot the vib-rotational distribution on the ground and excited state in Figs. 8 and 9, respectively. As can be seen in Fig. 8, for the $1^2A''$ PES the OH_2^+ products are mainly distributed in the large vibrational and median rotational quantum number; the shape looks like a “straw hat”; the vibrational distributions present typical population inversion. When D and T substitute for H, the distribution is significantly broader due to not only the vibration but also the rotation, and the vibrational population inversion is not changed. As op-

posed to the $1^2A''$ PES, the products are mainly distributed in the low vibrational and high rotational energy-level in the $1^2A'$ PES as shown in Fig. 9. The $v' = 1$ state has the greatest population for each E_C and no isotope substitution changes this result, it just expands the distribution area. This phenomenon is consistent with Polanyi’s rule,^[48] and this kind of vibrational inversion also exists in many other reactions.^[49–53] Because of energy conservation, for a given E_C , the maximum j' value reached in the distribution decreases as v' increases.

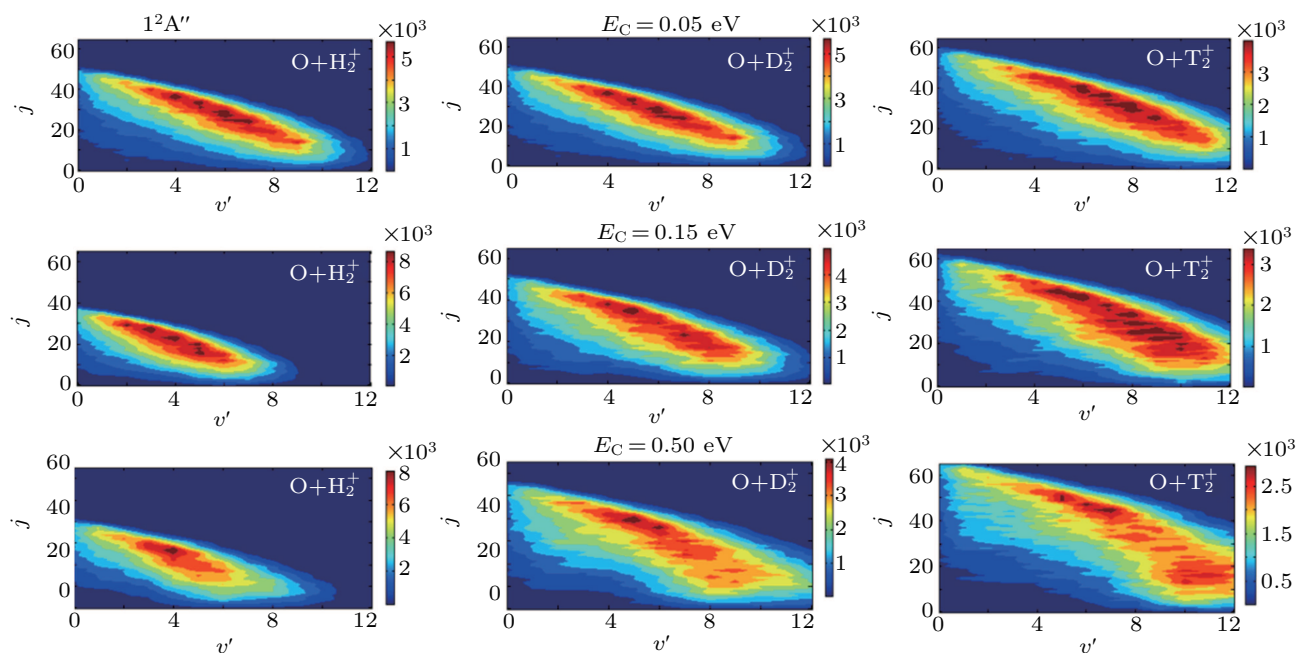


Fig. 8. Product ro-vibrational state-resolved distributions of $\text{O} + \text{H}_2^+ / \text{D}_2^+ / \text{T}_2^+ \rightarrow \text{OH}^+ + \text{H}, \text{OD}^+ + \text{D}, \text{OT}^+ + \text{T}$ reactions on the $1^2A''$ PES at collision energy of 0.05 eV, 0.15 eV, and 0.5 eV.

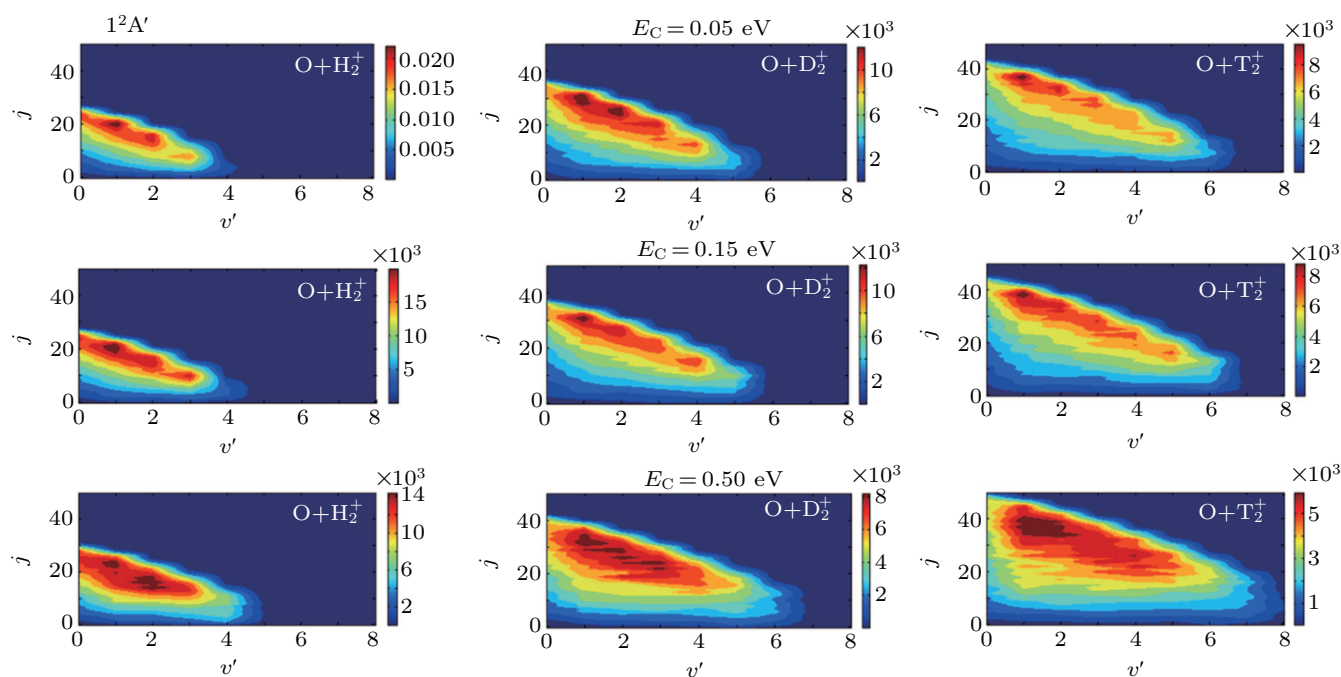


Fig. 9. Product ro-vibrational state-resolved distributions of $\text{O} + \text{H}_2^+ / \text{D}_2^+ / \text{T}_2^+ \rightarrow \text{OH}^+ + \text{H}, \text{OD}^+ + \text{D}, \text{OT}^+ + \text{T}$ reactions on the $1^2A'$ PES at collision energy of 0.05 eV, 0.15 eV, and 0.5 eV.

According to the analysis in Ref. [21], there are three reaction modes [(i) direct, (ii) non-direct (short-lived collision complexes), and (iii) complex (long-lived collision complexes)] in $O + H_2^+ \rightarrow OH^+ + H$ and $O + H_2^+ \rightarrow OH + H^+$ reactions. Because of the deeper potential well in $1^2A''$ PES, the formation of long-lived collision complexes occurs with a higher probability ($> 60\%$) over the whole range of collision energy. While for the $1^2A'$ PES the direct and non-direct mechanism' contribution to reactivity are always larger than the corresponding ones in reactions on the ground state, and the consequence is reverse for the complex mechanism, that is, there is a little difference in contribution between non-direct mechanism and complex mechanism for both reaction systems. In addition, since the potential wells in the two potential energy surfaces are too deep, neither of these reaction mechanisms can be fundamentally changed by isotopic substitution. Therefore, after D and T substitute for H, although there are some changes in the vibration transition state fraction of the products, the overall distribution shape remains unchanged.

3.3. Stereo-dynamics

Not only can the scalar properties be obtained from QCT calculations, but also the vector properties can be acquired by means of QCT.[37,54] We also study the effect of isotope substitution on the stereo-dynamic properties of the $O + H_2^+ \rightarrow OH^+ + H$ and $O + H_2^+ \rightarrow OH + H^+$ reactions.

In order to better present the influence of collision energy on vector properties, we choose the collision energy in a range of 0.01 eV–1.0 eV. We calculate the average rotational alignment factor $\langle P_2(\mathbf{k} \cdot \mathbf{j}) \rangle$, and the dependence of the product rotational alignment on collision energy is shown in Fig. 10. According to the analysis in Ref. [37], the closer to -0.5 the value of $\langle P_2(\mathbf{k} \cdot \mathbf{j}) \rangle$, the stronger the rotational polarization is. It can be seen in Fig. 10 that all the $\langle P_2(\mathbf{k} \cdot \mathbf{j}) \rangle$ values are larger than -0.25 , and as the collision energy increases, there are some changes in the $\langle P_2(\mathbf{k} \cdot \mathbf{j}) \rangle$ value, which means that the rotational angular momentum of the product has a certain alignment, and the collision energy has some effect on this alignment. Specifically, for the $1^2A''$ PES the $\langle P_2(\mathbf{k} \cdot \mathbf{j}) \rangle$ value monotonically becomes smaller as the collision energy increases, indicating that the alignment becomes somewhat stronger as the collision energy increases. Moreover, for $E_C > 0.03$ eV the isotope substitution will reduce the product rotational alignment. While for the $1^2A'$ PES, as the collision energy increases, the $\langle P_2(\mathbf{k} \cdot \mathbf{j}) \rangle$ value first becomes larger and then turns smaller, the inflection point is about $E_C = 0.2$ eV. For $E_C < 0.3$ eV the influence of isotope substitution is not clear, but for $E_C > 0.3$ eV, the isotope substitution promotes the product rotational alignment, which is opposite to the result for the ground state. The reason is that there is difference in reaction mechanism between the two systems, and these results are consistent with the product alignment prediction from the $P(\theta_r)$ distribution shown in Fig. 11,

which will be discussed later.

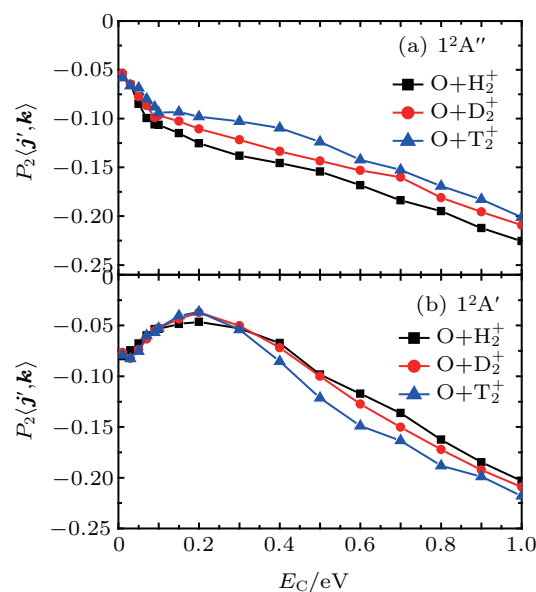


Fig. 10. Plots of product rotational alignment versus collision energy for (a) $O + H_2^+/D_2^+/T_2^+ \rightarrow OH^+ + H, OD^+ + D, OT^+ + T$ on the $1^2A''$ PES and (b) $O + H_2^+/D_2^+/T_2^+ \rightarrow OH + H^+, OD + D^+, OT + T^+$ on the $1^2A'$ PES.

Figure 11 shows the plots of calculated PDDCSs $[(2\pi/\sigma)(d\sigma_{00}/d\omega_t), (2\pi/\sigma)(d\sigma_{20}/d\omega_t)]$ versus both collision energy and scattering angle θ_t . It is known that PDDCS₀₀ correlates with the usual differential cross-section, and PDDCS₂₀ is the expectation value of the second Legendre moment $\langle P_2(\mathbf{k} \cdot \mathbf{j}) \rangle$. As can be seen, for the $1^2A''$ state there are both preferred forward scattering and backward scattering for all calculated PDDCS₀₀ that are peaked at 0° and 180° over the investigated energy range. The tendency is basically towards “forward”/“backward” symmetry, indicating that a complex reaction mechanism plays a leading role. Specifically, for the $O + H_2^+ \rightarrow OH^+ + H$ reaction the increase of collision energy leads to an overall enhancement in the forward scattering along with an overall reduction in the backward scattering, which means that the proportion of direct abstraction mechanism increases. The isotope substitution mostly does not change these distributions. The PDDCS₀₀ calculated for the $1^2A'$ state is not completely symmetric with respect to a forward scattering bias. Such a backward-forward asymmetry may probably occur because of the larger contribution of the direct mechanism than the contribution of the complex mechanism to the reactivity. As the collision energy increases, the degree of backward scattering becomes slightly stronger, which is consistent with the scenario in a direct abstraction reaction mechanism and becomes the same as the result in the $1^2A''$ state; the isotope substitution also has little effect on the angular distribution of the product. Finally, from the opposite trend shown by the PDDCS₂₀ and PDDCS₀₀ over the range of the scattering angle, it can be inferred that the product angular momentum \mathbf{j}' is aligned to the direction perpendicular to the reagent relative velocity \mathbf{k} .

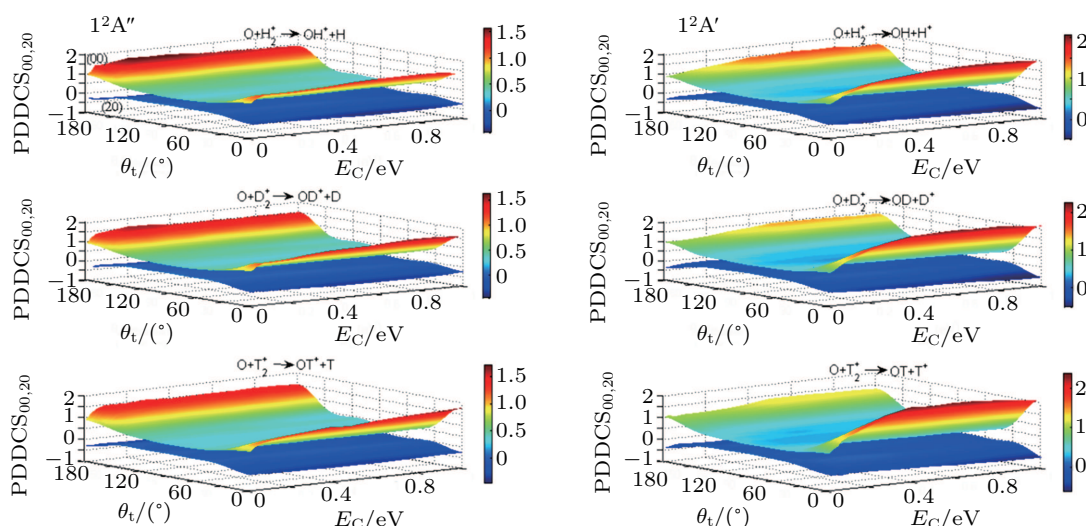


Fig. 11. Product rotational alignment as a function of collision energy for (a) $\text{O} + \text{H}_2^+/\text{D}_2^+/\text{T}_2^+ \rightarrow \text{OH}^+ + \text{H}$, $\text{OD}^+ + \text{D}$, $\text{OT}^+ + \text{T}$ on $1^2\text{A}''$ PES and (b) $\text{O} + \text{H}_2^+/\text{D}_2^+/\text{T}_2^+ \rightarrow \text{OH} + \text{H}^+$, $\text{OD} + \text{D}^+$, $\text{OT} + \text{T}^+$ on $1^2\text{A}'$ PES.

To obtain a better graphical representation of the influence of isotope substitution on the polarization of the products from the reaction, we plot the $P(\theta_r)$ distribution, which describes the $\mathbf{j}'\text{-}\mathbf{k}$ vector correlation with $\mathbf{j}' \cdot \mathbf{k} = \cos \theta_r$. As shown in Fig. 12, all three reactions occurring in the $1^2\text{A}''$ state illustrate the symmetric $P(\theta_r)$ distributions peaked at $\theta_r = 90^\circ$, indicating that the product angular momentum \mathbf{j}' tends to align to the direction perpendicular to \mathbf{k} . Moreover, as the collision energy increases, there appears a contraction in the calculated $P(\theta_r)$ distributions with the peak moving upward, thus suggesting that the product alignment becomes stronger at high collision energy. For the $1^2\text{A}'$ state all three reactions exhibit lower and broader distributions than the corresponding ones in

the $1^2\text{A}''$ state, which implies a rather weaker product alignment in the excited state. This can be attributed to the larger product rotational angular momentum that comes from the initial orbital angular momentum \mathbf{L} in the $1^2\text{A}''$ state; the products will retain a greater initial direction “memory” for the reactions in $1^2\text{A}''$ state. In addition at the beginning there is a decrease in the $P(\theta_r)$ peak value as the collision energy increases in the $1^2\text{A}'$ state, which is consistent with the $\langle P_2(\mathbf{k} \cdot \mathbf{j}) \rangle$ result. For the $1^2\text{A}''$ state the isotope substitution induces the $P(\theta_r)$ distribution to expand, that is, it weakens the product alignment, while for $1^2\text{A}'$ state, there is a slight enhancement in the product alignment.

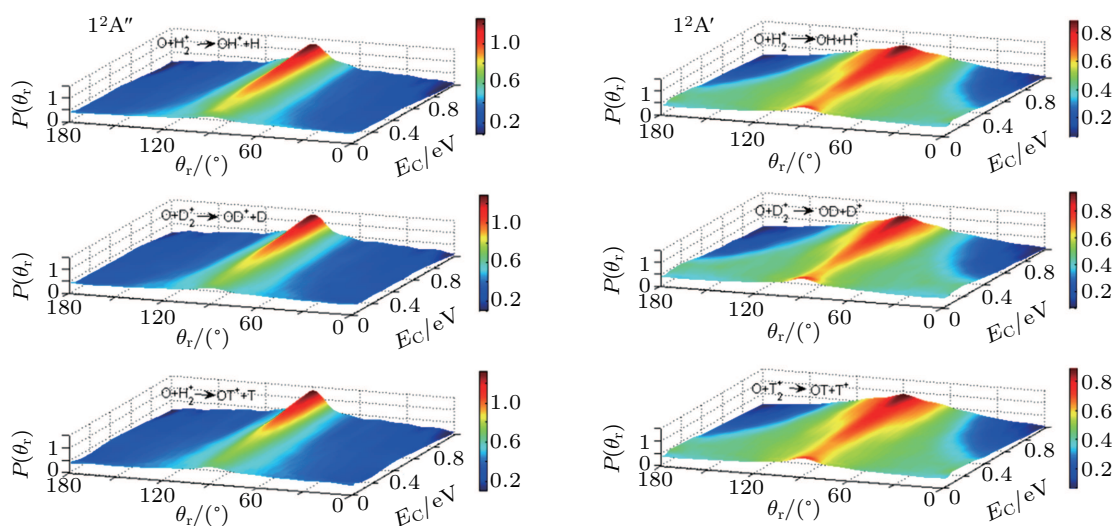


Fig. 12. Product rotational alignments as a function of collision energy for (a) $\text{O} + \text{H}_2^+/\text{D}_2^+/\text{T}_2^+ \rightarrow \text{OH}^+ + \text{H}$, $\text{OD}^+ + \text{D}$, $\text{OT}^+ + \text{T}$ on $1^2\text{A}''$ PES and (b) $\text{O} + \text{H}_2^+/\text{D}_2^+/\text{T}_2^+ \rightarrow \text{OH} + \text{H}^+$, $\text{OD} + \text{D}^+$, $\text{OT} + \text{T}^+$ on $1^2\text{A}'$ PES.

As mentioned in Ref. [21], for the $\text{O} + \text{H}_2^+ \rightarrow \text{OH}^+ + \text{H}$ reaction in the $1^2\text{A}''$ PES, the complex (long-lived collision complexes) mechanism is dominant ($> 60\%$), and with the increase of collision energy, more and more non-direct (short-

lived collision complexes) reaction trajectories are converted into the direct reaction trajectories. The product rotational alignment becomes stronger and stronger, which is also consistent with the product rotational alignment of the HL–L mass

combination reaction^[37,55] While for the $\text{O} + \text{H}_2^+ \rightarrow \text{OH} + \text{H}^+$ reaction in the $1^2A'$ PES, the complex (long-lived collision complexes) mechanism is not dominant ($< 45\%$) in a range of 0.01 eV–0.5 eV, and the direct mechanism has a larger contribution to reactivity than the scenario for the reaction in the $1^2A''$ PES, but the long-lived collision complexes have somewhat larger average lifetime than those in the $1^2A'$ PES. Therefore, the value of $\langle P_2(\mathbf{k} \cdot \mathbf{j}) \rangle$ in the excited state is larger than in the ground state at the same energy, and the peak value of the $P(\theta_r)$ distribution is also broadened.

The isotopic variant directly leads the reagent $\text{O}-\text{H}_2^+$ relative velocity to be greatest in $\text{O}-\text{D}_2^+$ and $\text{O}-\text{T}_2^+$ at the same collision energy. Therefore, when D or T substitutes for H, it will take longer time to produce products, the loss of initial direction is more serious, and the polarization strength is weakened, which is consistent with the result of $1^2A''$ PES.

For the excited state it is a little bit more complicated. Because the saddle point configuration is linear, it is very hard to make products have a regular alignment at small collision energy. This irregularity increases as the collision energy slightly increases, so at the beginning of the $\langle P_2(\mathbf{k} \cdot \mathbf{j}) \rangle$ the values become larger, and the isotopic substitution does not weaken it. As the collision energy increases further, the $\langle P_2(\mathbf{k} \cdot \mathbf{j}) \rangle$ value becomes smaller, and the product rotational alignment becomes stronger, this is easier to understand. Like the effect of isotope substitution on the ICSs, the effects of isotope substitution on $\langle P_2(\mathbf{k} \cdot \mathbf{j}) \rangle$ and $P(\theta_r)$ of the excited state are also different from that of the ground state, which can also be attributed to the different ZPE effects on these two PESs.

The dihedral angle distributions $P(\phi_r)$ describing the correlations are depicted in Fig. 13. Because ϕ_r defines the dihedral angle between the planes consisting of $\mathbf{k}-\mathbf{k}'$ and $\mathbf{k}-\mathbf{j}'$, the $P(\phi_r)$ distribution correlates to the $\mathbf{k}-\mathbf{k}'-\mathbf{j}'$ vector and

can provide stereo-dynamical information about both product alignment and product orientation. Figure 13 shows the $P(\phi_r)$ distributions for the ground (the left column) and excited (the right column) state for all the isotope substitution reactions at the three collision energy values of 0.05, 0.15, and 0.5 eV, respectively. Clearly, the $P(\phi_r)$ distributions are similar because of the similar properties of both PESs. All the $P(\phi_r)$ distributions illustrate asymmetric properties with respect to the scattering $\mathbf{k}-\mathbf{k}'$ plane, with one large and one small peak appearing at $\phi_r = 90^\circ$ and $\phi_r = 270^\circ$, respectively. This feature produces two important messages: one is alignment, *i.e.*, all products tend to align along the direction of y axis which is perpendicular to the scattering plane, and the other is orientation, *i.e.*, product molecules tend to orient to the positive direction of y axis. In other words, the product molecules prefer an anticlockwise rotation (see from the right side of the plane) in the plane parallel to the scattering plane. For both states, as collision energy increases, the peak appearing at $\phi_r = 90^\circ$ obviously becomes higher and higher, while for the peaks appearing at $\phi_r = 270^\circ$ the increase is not obvious. That is, the increase of collision energy enhances the orientation along the $+y$ direction, and this effect is more pronounced for the $1^2A''$ state. In addition, it can be seen in Fig. 13 that the isotope substitution has little influence on the orientation for these two states. According to the discussion in Ref. [33], the difference in orientation degree is mainly due to the different harmonic ZPE of the reactant molecule, which will induce the different effective potential barrier height or well depth. For the reactions in this study, because the potential wells are very deep, the difference of the harmonic ZPE from the isotopic substitution plays a very small role, thus the influence of isotope substitution on the orientation is quite small.

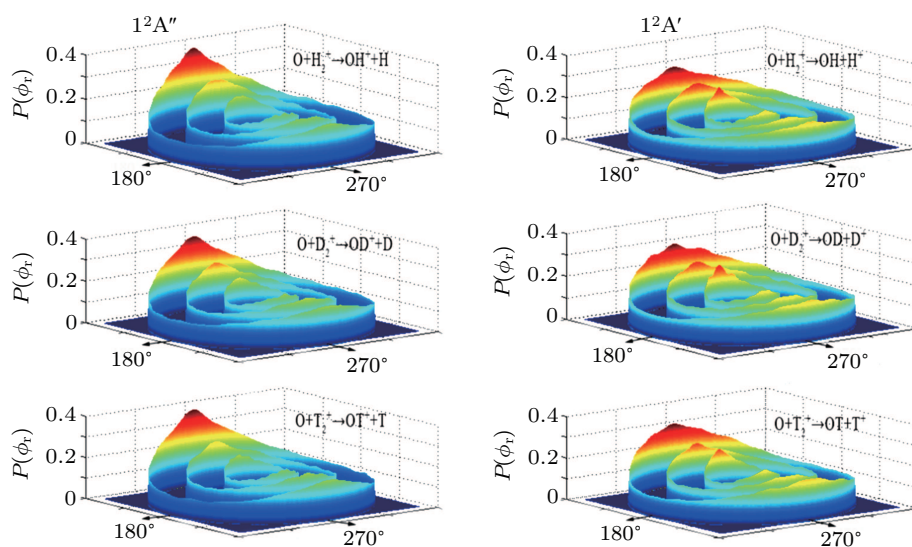


Fig. 13. $P(\phi_r)$ distributions as a function of dihedral angle ϕ_r at three collision energy values of 0.05, 0.15, and 0.5 eV (from inner to outer) for $\text{O} + \text{H}_2^+/\text{D}_2^+/\text{T}_2^+ \rightarrow \text{OH} + \text{H}$, $\text{OD} + \text{D}$, $\text{OT} + \text{T}$ on $1^2A''$ PES and $\text{O} + \text{H}_2^+/\text{D}_2^+/\text{T}_2^+ \rightarrow \text{OH} + \text{H}^+$, $\text{OD} + \text{D}^+$, $\text{OT} + \text{T}^+$ on $1^2A'$ PES.

In order to validate more information about the angular momentum polarization, we depict them in the form of polar plots θ_r and ϕ_r averaged over all scattering angles in Figs. 14 ($1^2A''$) and 15 ($1^2A'$). It can be seen that for all $P(\theta_r, \phi_r)$ distributions, there are two peaks: the large one is at $(\theta_r = 90^\circ, \phi_r = 90^\circ)$ and the small one is at $(\theta_r = 90^\circ, \phi_r = 270^\circ)$. This

further supports the fact that products align along the direction of the y axis and orient to the positive direction of the y axis. It also clearly shows the collision energy will obviously enhance the orientation for the $1^2A''$ state more than for $1^2A'$ state and will have little influence from the isotope substitution, which is associated with the above-mentioned findings.

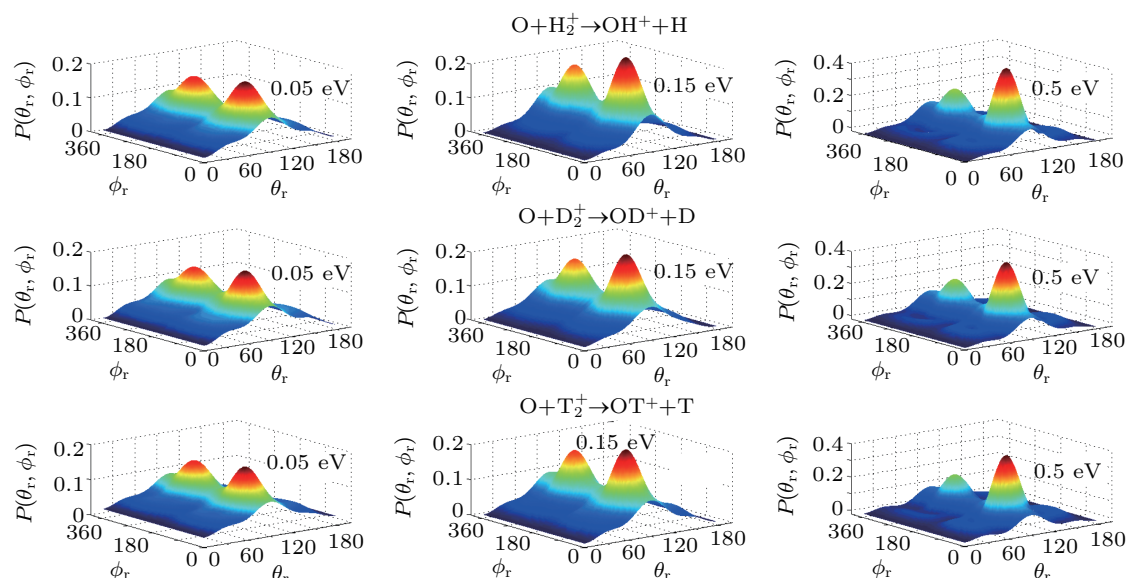


Fig. 14. Polar plots of $P(\theta_r, \phi_r)$ distribution at three collision energy values of 0.05, 0.15, and 0.5 eV (from left to right) for $O + H_2^+/D_2^+/T_2^+ \rightarrow OH^+ + H, OD^+ + D, OT^+ + T$ reactions on $1^2A''$ PES.

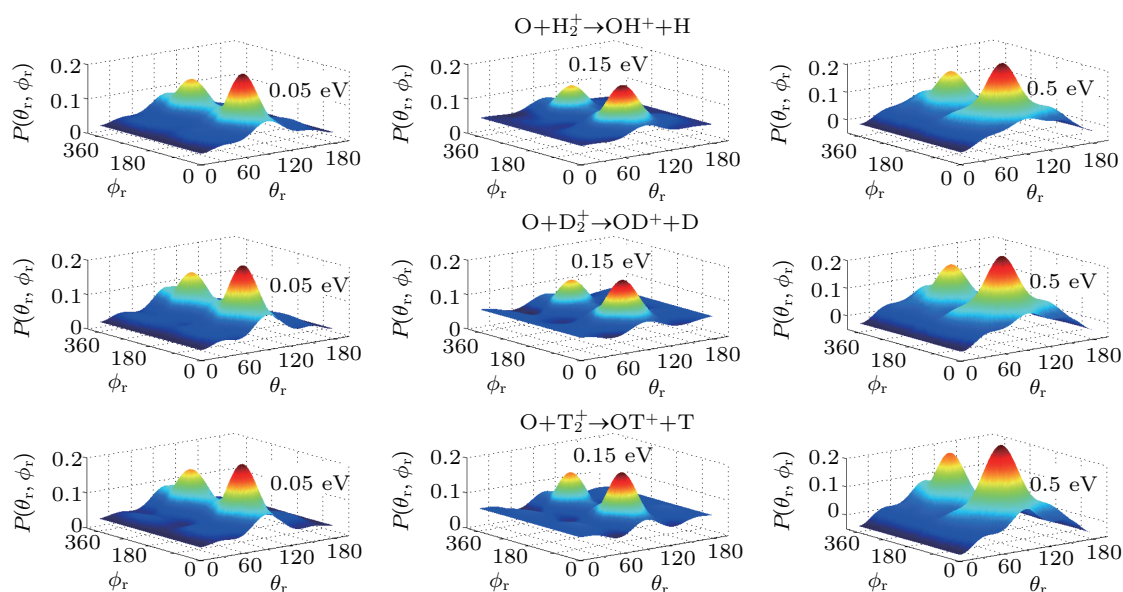


Fig. 15. Polar plots of $P(\theta_r, \phi_r)$ distribution at three collision energy values of 0.05, 0.15, and 0.5 eV (from left to right) for $O + H_2^+/D_2^+/T_2^+ \rightarrow OH^+ + H, OD^+ + D, OT^+ + T$ reactions on $1^2A'$ PES.

4. Summary

Quantum wave packet and QCT are calculated to investigate the effect of isotopic substitution on the dynamics of the reactions. We find for $J = 0$, the reaction probabilities obtained by the two calculation methods for both reactive systems are in fairly good agreement. Although the isotopic substitution has no obvious influence on the integral cross-section,

it has an obvious influence on the reaction probability for high collision energy: it will increase the reaction probability of reaction in the $1^2A''$ PES but reduce the reaction probability of reactions in the $1^2A'$ PES. Moreover, the vibrational and rotational distributions are broadened when D and T substitute for H. The calculated value of $\langle P_2(\mathbf{k} \cdot \mathbf{j}) \rangle$ shows that at high collision energy, the isotope substitution will reduce and enhance

the product rotational alignment for $1^2A''$ state and $1^2A'$ state, respectively. The PDDCS results show that products from the two electronic states have a similar scattering behavior: the forward scattering is stronger for the excited state, but the isotope substitution will weaken the backward scattering behavior for the $1^2A'$ state. Finally, the isotope substitution will slightly enhance the product alignment to the direction perpendicular to k , but it has little effect on the product orientation.

Acknowledgment

The authors are very grateful to Prof. Miguel Paniagua for providing the potential energy surface, and also to Prof. Han for providing the code.

References

- [1] Duley W W and Williams D A 1986 *Mon. Not. R. Astr. Soc.* **223** 177
- [2] Xu Y, Xiong B, Chang Y C and Ng C Y 2012 *J. Chem. Phys.* **137** 241101
- [3] Martínez R, Millán J and González M 2004 *J. Chem. Phys.* **120** 4705
- [4] González M, Gilibert M, Aguilar A and Sayós R 1993 *J. Chem. Phys.* **98** 2927
- [5] Martínez R, Sierra J D, Gray S K and González M 2006 *J. Chem. Phys.* **125** 164305
- [6] Martínez R, Sierra J D and González M 2005 *J. Chem. Phys.* **123** 174312
- [7] Martínez R, Lucas J M, Giménez X, Aguilar A and González M 2006 *J. Chem. Phys.* **124** 144301
- [8] Xu W W, Li W L, Lv S J, Zhai H S, Duan Z X and Zhang P Y 2012 *J. Phys. Chem. A* **116** 10882
- [9] Yuan M L and Li W T 2019 *Acta Phys. Sin.* **68** 083401 (in Chinese)
- [10] Pablo G, Fermín H L and Miguel G 2013 *J. Phys. Chem. A* **117** 5393
- [11] Gamallo P, Defazio P and González M 2011 *J. Phys. Chem. A* **115** 11525
- [12] Chu T S, Lu R F, Han K L, Tang X N, Xu H F and Ng C Y 2005 *J. Chem. Phys.* **122** 244322
- [13] Tang X N, Houchins C, Lau K C, Ng C Y, Dressler R A, Chiu Y H, Chu T S and Han K L 2007 *J. Chem. Phys.* **127** 164318
- [14] McClure D J, Douglass C H and Gentry W R 1977 *J. Chem. Phys.* **67** 2362
- [15] Paniagua M, Martínez R, Gamallo P and González M 2014 *Phys. Chem. Chem. Phys.* **16** 23594
- [16] Werner H J and Knowles P J 1988 *J. Chem. Phys.* **89** 5803
- [17] Knowles P J and Werner H J 1988 *Chem. Phys. Lett.* **145** 514
- [18] Gamallo P, Defazio P, Gonzalez M, Paniagua M and Petrongolo C 2015 *Phys. Chem. Chem. Phys.* **17** 23392
- [19] Zhang Y, Cao E, Gao S, Huang X, Meng Q and Song Y 2017 *Int. J. Quant. Chem.* **117** e25343
- [20] Zhang A J, Zang K L, Jia J F, Wu H S, Wang Y and Zhao G G 2017 *Chem. Phys. Lett.* **676** 77
- [21] Martínez R, Paniagua M, Mayneris-Perxachs J, Gamallo P and González M 2017 *Phys. Chem. Chem. Phys.* **19** 3857
- [22] Assafrão D and Mohallem J R 2007 *J. Phys. B* **40** F85
- [23] Kimura T, Matsushita T, Ueda K, Tamura K and Takagi S 2001 *J. Theor. Anal. Calc.* **64** 231
- [24] Chen M D, Han K L and Lou N Q 2002 *Chem. Phys. Lett.* **357** 483
- [25] Zhao J, Xu Y and Meng Q T 2009 *J. Phys. B* **42** 165006
- [26] Chu T 2010 *J. Comput. Chem.* **31** 1385
- [27] Zhang J, Gao S B, Song Y Z and Meng Q T 2015 *Int. J. Quantum Chem.* **115** 231
- [28] Chu T S, Zhang Y and Han K L 2006 *Int. Rev. Phys. Chem.* **25** 201
- [29] Li W T, Yu W and Yao M H 2018 *Acta Phys. Sin.* **67** 103401 (in Chinese)
- [30] Yao L, Ju L P, Chu T S and Han K L 2006 *Phys. Rev. A* **74** 062715
- [31] Davidsson J and Nyman G 1990 *J. Chem. Phys.* **92** 2407
- [32] Nyman G and Davidsson J 1990 *J. Chem. Phys.* **92** 2415
- [33] Bowman J M, Gazdy B and Sun Q 1989 *J. Chem. Phys.* **91** 2859
- [34] Truhlar D G 1979 *J. Phys. Chem.* **83** 188
- [35] Bonnet L and Rayez J C 2004 *Chem. Phys. Lett.* **397** 106
- [36] Varandas A J C 2007 *Chem. Phys. Lett.* **439** 386
- [37] Han K L, He G Z and Lou N Q 1996 *J. Chem. Phys.* **105** 8699
- [38] Zhang X and Han K L 2006 *Int. J. Quantum Chem.* **106** 1815
- [39] Lin S Y, Han K L and Zhang J Z H 2000 *Chem. Phys. Lett.* **324** 122
- [40] Zhao J, Xu Y and Meng Q T 2010 *Chin. Phys. B* **19** 063403
- [41] Zhao J and Luo Y 2011 *Chin. Phys. B* **20** 043402
- [42] Zhang W, Li Y, Xu X and Chen M 2010 *Chem. Phys.* **367** 115
- [43] Chu T S, Han K L and Schatz G C 2007 *J. Phys. Chem. A* **111** 8286
- [44] Li J and Guo H 2013 *Chin. J. Chem. Phys.* **26** 627
- [45] Song H, Li A and Guo H 2016 *J. Phys. Chem. A* **120** 4742
- [46] Zhao J 2013 *J. Chem. Phys.* **138** 134309
- [47] Murray C, Pearce J K, Rudić S, Retail B and Orr-Ewing A J 2005 *J. Phys. Chem. A* **109** 11093
- [48] Polanyi J C 1987 *Angew. Chem. Int. Ed.* **26** 952
- [49] Yue D G, Zhang L L, Zhao J, Song Y Z and Meng Q 2019 *Comput. Theor. Chem.* **1155** 82
- [50] Meng Q 2018 *Chem. Phys.* **509** 131
- [51] Aldegunde J, Jambriña P G, González Sanchez L, Herrero V J and Aoiz F J 2015 *J. Phys. Chem. A* **119** 12245
- [52] Zhang L, Gao S, Song Y and Meng Q 2018 *J. Phys. B* **51** 065202
- [53] Sáez Rábanos V, Verdasco J E, Aoiz F J and Herrero V J 2016 *Phys. Chem. Chem. Phys.* **18** 13530
- [54] Aoiz F J, Brouard M and Enriquez P A 1996 *J. Chem. Phys.* **105** 4964
- [55] Wang M L, Han K L and He G Z 1998 *J. Chem. Phys.* **109** 5446